ISSN 1674-1056
http://cpb.iphy.ac.cn
http://iopscience.iop.org/cpb
中国物理 B
Chinese Physics
中国物理
Chinese Physics B

Temporal and spatial evolution of air-spark switch plasmaby the Mach-Zehnder interferometer

Jie Huang(黄杰), Lin Yang(杨林), Hongchao Zhang(张宏超), Lei Chen(陈磊), Xinying Wu(吴先映)

Citation: Chin. Phys. B . 2019, 28(5): 055202. **doi:** 10.1088/1674-1056/28/5/055202
Journal homepage: http://cpb.iphy.ac.cn; http://iopscience.iop.org/cpb

What follows is a list of articles you may be interested in

Electrical and thermal characterization of near-surface electrical discharge plasma actuation driven by radio frequency voltage at low pressure

Zhen Yang(杨臻), Hui-Min Song(宋慧敏), Di Jin(金迪), Min Jia(贾敏), Kang Wang(王康)

Chin. Phys. B . 2018, 27(8): 085205. **doi:** 10.1088/1674-1056/27/8/085205

Electric ignition energy evaluation and the energy distribution structure of energy released in electrostatic discharge process

Qingming Liu(刘庆明), Jinxiang Huang(黄金香), Huige Shao(邵惠阁), Yunming Zhang(张云明)

Chin. Phys. B . 2017, 26(10): 105202. **doi:** 10.1088/1674-1056/26/10/105202

Conversion of an atomic to a molecular argon ion and low pressure argon relaxation

M N Stankov, A P Jovanović, V Lj Marković, S N Stamenković

Chin. Phys. B . 2016, 25(1): 015204. **doi:** 10.1088/1674-1056/25/1/015204

Current-voltage characteristics of hydrogen DC plasma torches with different sizes in an external axial magnetic field

Ma Jie, Wen Guang-Dong, Su Bao-Gen, Yang Yi-Wen, Ren Qi-Long

Chin. Phys. B . 2015, 24(6): 065205. **doi:** 10.1088/1674-1056/24/6/065205

Characteristics of dual-frequency capacitively coupled SF_6/O_2 plasma and plasma texturing of multi-crystalline silicon

Xu Dong-Sheng, Zou Shuai, Xin Yu, Su Xiao-Dong, Wang Xu-Sheng

Chin. Phys. B . 2014, 23(6): 065201. **doi:** 10.1088/1674-1056/23/6/065201

Temporal and spatial evolution of air-spark switch plasma investigated by the Mach–Zehnder interferometer

Jie Huang(黄杰)[1,2], Lin Yang(杨林)[2,†], Hongchao Zhang(张宏超)[3], Lei Chen(陈磊)[2], and Xianying Wu(吴先映)[1]

[1] College of Nuclear Science and Technology, Beijing Normal University, Beijing 100875, China
[2] Institute of Electronic Engineering, China Academy of Engineering Physics, Mianyang 621900, China
[3] Nanjing University of Science and Technology, Nanjing 210094, China

(Received 19 December 2018; revised manuscript received 4 March 2019; published online 4 April 2019)

An air-spark switch plasma was diagnosed by the Mach–Zehnder laser interferometer with ultra-high spatial and temporal resolution. The interferograms containing plasma phase shift information at different time were obtained. The phase shift distributions of the plasma were extracted by numerically processing the interferograms. The three-dimensional (3D) electron density distributions of the air-spark switch plasma were then obtained. The working process of the air-spark switch was described by analyzing the temporal and spatial evolution of the plasma electron density.

Keywords: air-spark switch, Mach–Zehnder laser interferometer, arc channel, electron density

PACS: 52.75.Kq, 52.80.–s, 07.60.Ly **DOI:** 10.1088/1674-1056/28/5/055202

1. Introduction

Gas spark switches as the key component are widely used in pulsed power generators, pulse modulation networks, vacuum electron devices, particle accelerators, and other high pulsed power devices.[1–4] They have extraordinary capabilities that are well suited for applications that require switching of very high voltage, long life, and rather high currents. The main purpose of researching gas spark switches is to achieve high reliability. At the same time, high reliability of gas spark switch is also the guarantee for the safe operation of pulse power equipment. At present, the research on gas spark switch mainly focuses on the numerical calculation and experimental research of its circuit characteristic parameters, the numerical simulation of the main arc of the switching arc and the electrode ablation.[5–8] With the development of plasma diagnostic techniques, the accurate diagnosis of plasma parameters of gas spark switches has become possible. These new plasma diagnostic techniques help us to better understand the working process of gas spark switches.[9,10]

The air-spark switch is a kind of gas spark switch that uses air as the insulating medium. The electron density distribution and evolution of the air-spark switch discharge plasma have a significant effect on the operating process of the air-spark switch. It is well known that the air-spark switch discharge is a transient and complicated physical process. Generally, the major physical processes of discharge contain two stages, plasma formation and plasma expansion. However, there is no clear threshold for the two stages. Once the plasma is produced, it will expand in the background gas and the shock waves will form because of the steep density gradient.[11,12] Many works have been carried out to comprehend the processes of plasma formation and plasma expansion in the background gap. Zhang *et al.* studied laser induced plasma in air using the laser interferometry and a three-dimensional (3D) electron density profile was obtained.[13,14] Hairlal *et al.* used laser shadowgraph and fluid simulation to study the shock wave propagation, estimating the pressure and the velocity of the shock front.[15] Yang *et al.* studied laser induced copper plasmas in air using fast spectral imaging and two-color laser interferometry, and the density profiles of Cu atoms and electrons were obtained.[16]

Obtaining the exact parameters of air-spark switch plasma is the key to understanding the working process of the air-spark switch, but it is a challenge because of the rapid changes of the plasma parameters in time and space. Fortunately, the laser interference imaging can "freeze" the plasma, obtain and analyze the transient parameters of the plasma by numerical processing the interferograms. In this paper, the Mach–Zehnder (M–Z) laser interferometer with laser wavelength 532 nm is used to diagnose the gas spark switch plasma. The interferograms containing plasma information are obtained, and the electron density distribution of the plasma is presented by numerical processing the interferograms. The spatiotemporal evolution of the plasma electron density is analyzed.

2. Theory and assumptions

Low temperature plasma is mainly composed of electrons, ions, and neutral atoms.[17] Different types of particles have different contributions to the refractive index of the plasma. So the refractive index of plasma can be written as[14]

$$n-1=-\frac{e_0^2\lambda^2 N_{\rm e}}{8\pi^2\varepsilon_0 m_{\rm e}c^2}+\sum_k\left(A_k+\frac{B_k}{\lambda^2}\right)\frac{N_k}{N_{\rm A}}, \qquad (1)$$

†Corresponding author. E-mail: fuyunyufeng@163.com

© 2019 Chinese Physical Society and IOP Publishing Ltd

where n is the refractive index of the plasma, λ is the wavelength of the probe laser beam, e_0 is the elementary charge, m_e is the electronic mass, ε_0 is the dielectric constant, c is the speed of light in vaccum, N_A is the Avogadro constant. N_e is the number density of free electron, and N_k is the number density of particle of kind k. A_k and B_k denote the gas-specific constants for these particles. In Eq. (1), the first term is the contribution from free electrons and the second term from heavy particles (atoms and ions).

Generally, we can obtain the accurate plasma electron density by measuring the refractive index distributions of plasma at two separate wavelengths.[18] However, in the plasma, the refractive index is primarily a function of the electron density, which is the main plasma parameter determined by refractive index measurements. In particular, when the electron density is above 2×10^{19} cm^{-3}, the influence of electrons on the refractive index is dominants and the heavy particle influence is neglected entirely.[19] For air-switched plasma, in the arc-column region between the electrodes, we assume that the plasma is fully ionized. At the same time, we ignore the effect of ions on the refractive index. Thus the electron density N_e can be calculated from a refractive index distribution at a single probing wavelength λ

$$N_e = \frac{8\pi^2\varepsilon_0 m_e c^2}{e_0^2\lambda^2}(n-1). \tag{2}$$

Laser interferometry measures the change in refractive index of a tested plasma. When the probing laser beam passes the plasma, the phase shift $\Delta\varphi$ will be recorded in the interferograms.[19] The $\Delta\varphi$ can be expressed as[16]

$$\Delta\varphi = \frac{2\pi}{\lambda}\int_{z_1}^{z_2}\{n-n_0\}\,\mathrm{d}l, \tag{3}$$

where $\Delta\varphi$ is the phase shift of the probing laser beam passed through the plasma, n is the refractive index of the plasma, n_0 is the refractive index of air ($n_0 = 1.0003$), and l is the propagation path of the probing laser beam in the plasma.

For axisymmetric plasma systems, digitizing the interferograms and performing the inverse Abel transformation, we can reconstruct the spatial distribution of the refractive index, and then the spatial and temporal distribution of the electron density in the plasma can be obtained. The inverse Abel transformation can be expressed as follows:

$$n-n_0 = -\frac{\lambda}{\pi}\int_r^R \frac{\mathrm{d}\Delta\varphi(x)/\mathrm{d}x}{\sqrt{x^2-y^2}}\mathrm{d}x. \tag{4}$$

There is a simple approximation formula: if the electron density of the plasma is much lower than the critical electron density, then the phase shift $\Delta\varphi$ is proportional to λ[20]

$$\Delta\varphi = 4.46\times10^{-14}\lambda\int_0^l N_e\mathrm{d}l. \tag{5}$$

For a probing laser beam with wavelength of 532 nm, the critical electron density is 4×10^{21} cm^{-3}. According to previous studies, the critical electron density is much larger than the electron density of the air-spark switching plasma.[21] Therefore, the electron density distribution of the air-spark switching plasma can be calculated according to the approximation formula.

3. Experimental setup

The experimental setup is shown in Fig. 1. The output laser (wavelength 1064 nm) of a Q-switch Nd: YAG laser is frequency-doubled with low efficiency (15%) to provide a probe pulse laser ($\lambda = 532$ nm), and the full width at half maximum (FWHM) of the laser pulse is about 7 ns. Then the probe pulse laser passes through an aperture that is used to adjust the intensity of the laser beam. A sample optical path delay system composed of two mirrors is used to adjust the direction of propagation of the laser beam. Then, the laser beam is separated into two beams by the Mach–Zehnder interferometer. The plasma is situated at one arm of the Mach–Zehnder interferometer. The laser beam which passes through the plasma is called the probe beam and the other beam that does not pass through the plasma is called the reference beam. The probe beam passed through the plasma interferes with the reference beam and produces an interferogram image on the charge coupled device (CCD) camera. The CCD camera is connected with a personal computer, which is used to display and store the interferograms in real time. To improve the spatial resolution of the device, a microscope (magnification of 10×) is installed on each arm of the interferometer. So, the spatial resolution of the interferometer can reach 5 μm (for one pixel). The temporal resolution of the interferometer is determined by the FWHM of the laser pulse that is 7 ns. In order to eliminate the effects of plasma luminescence and other stray light and improve the contrast of the interferograms, a band-pass filter ($\lambda = 532$ nm, FWHM = 1 nm) is used in front of the CCD camera. To accurately "freeze" the plasma and obtain an interferogram containing plasma information, the digital delay pulse generator (DG535) is used to control the time series of the laser (Nd: YAG), the high voltage power supply (HV Power Supply), and the CCD camera.

In our experiments, for the convenience of observation and research, we chose a two-electrode gas switch and simplified the switch structure as a two-tip discharge structure, whose schematic diagram is shown in Fig. 1. The plasma was generated between two needle-type copper electrodes, the gap between them was 2 mm. The air-spark switch was ignited in self-breakdown mode. The output voltage amplitude of the high-voltage pulse power supply was −10 kV, and the discharge duration was 3 μs. The typical waveforms of the air-spark switch ignited in air are shown in Fig. 2.

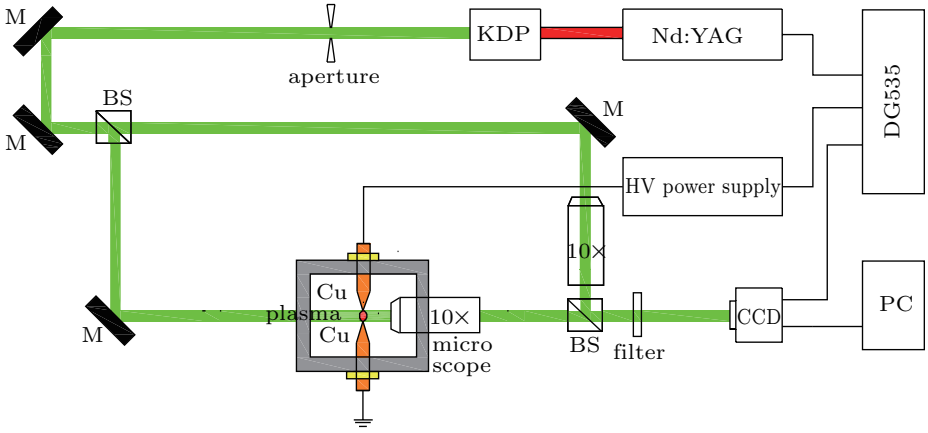


Fig. 1. The experimental set for laser interferometry to diagnose the air-spark switching plasma. KDP: potassium dihydrogen phosphate, M: mirror, BS: beam splitter, CCD: CCD camera, PC: personal computer, DG645: digital delay pulse generator, HV power supply: high voltage pulse power supply.

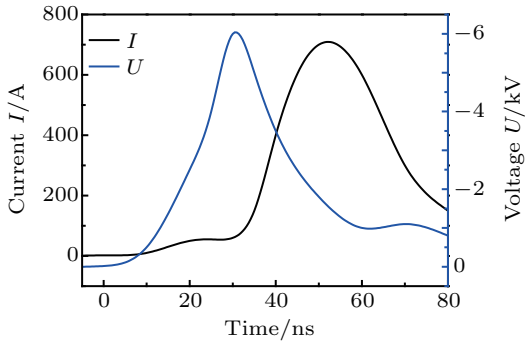


Fig. 2. Waveforms of the current I and voltage U of an air-spark switch ignited in air.

4. Results and discussions

4.1. Interferograms

All of our experiments are performed in air. In our experiments, the ignition of the air-spark switch is in the single ignition mode. Although the experimental device can obtain only one interferogram in a single discharge of air-spark switch, the stability of the high-voltage pulsed power supply ensures that the time jitter of the discharge is very small (< 5 ns). At the same time, the air-spark switch is simplified to a two-needle-type-electrodes discharge structure such that each discharge is produced at the tip of the needle. For the two reasons above, the good reproducibility of the experiment can be ensured. Time series is controlled by using DG535, the interferograms of different delay time can be obtained. The temporal and spatial evolution of the plasma electron density can be studied by processing the interferograms.

Typical interferograms obtained at different delay time are shown in Fig. 3. The interferogram in Fig. 3(a) is obtained when the electrode gap has just been broken down and the current in the electrode gap has just been generated. For the convenience of record and research, the moment of obtaining this interferogram is defined as time zero. In the interferogram in Fig. 3(a), the interference fringes are shifted in a small area of the electrode gap, especially near the cathode, which indicates that there is an electron cloud near the cathode. The interferogram in Fig. 3(b) is obtained at $t = 10$ ns. The plasma channel completely forms and a typical columnar plasma region can be observed in the electrode gap.

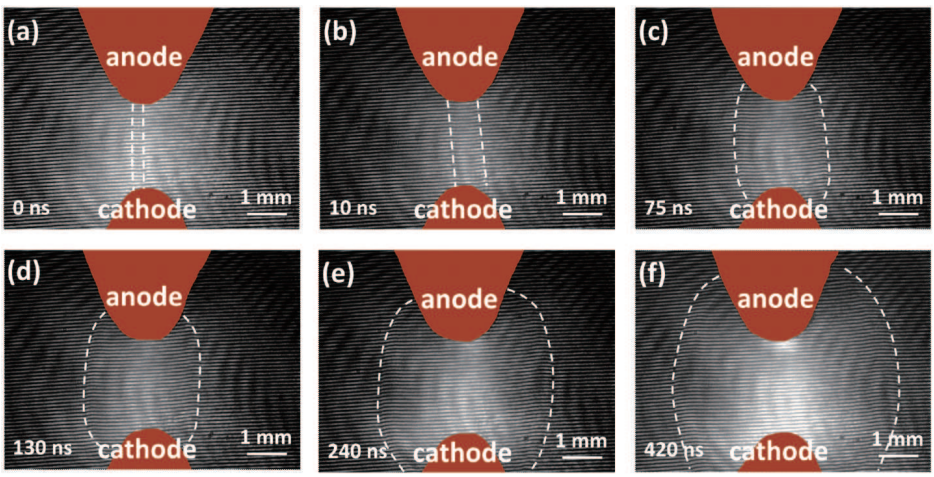


Fig. 3. The interferograms of air-spark switch discharge plasma obtained at different delay time: (a) 0 ns, (b) 10 ns, (c) 75 ns, (d) 130 ns, (e) 240 ns, (f) 420 ns.

The interferogram in Fig. 3(c) is obtained at $t = 75$ ns. A spherical plasma region is observed, which indicates that the plasma has expanded into the surrounding air. From the interferogram in Fig. 3(d) that is obtained at $t = 130$ ns, we find that the plasma has expanded into the surrounding air completely. The interferograms in Figs. 3(e) and in 3(f) are obtained at $t = 240$ ns and $t = 420$ ns, respectively. The plasma area then becomes bigger and bigger.

4.2. Phase shift distribution

The interferograms obtained in the experiments have a high quality and can be used to calculate the phase shift of the interference fringes. The phase shift ($\Delta\varphi$) is the most critical parameter to calculate the electron density of the plasma. First, the interferograms are digitized and low pass filtered. We perform a fast Fourier transformation (FFT) analysis to extract the phase shift from the fringe pattern, select the phase main value of the interferograms in the frequency domain, and then perform inverse FFT transformation to obtain the phase distribution.[22] Air-spark switching plasmas have high electron densities and density gradients. When the plasma expands into the atmosphere, high-speed diffusion of plasma always induces shock waves, which will cause phase shift discontinuity. The resulting phase is wrapped into interval $[-\pi, +\pi]$. To obtain a continuous phase, a phase unwrapping algorithm that uses graph cuts is applied.

To avoid confusion, we consider the condition when the arc channel is a column, and the electron density distribution is radially symmetric. The electron density is uniform in the z direction as shown in Fig. 4. The obtained phase shift distribution is shown in Fig. 5 as a false color image. According to formula (1), we know that the refractive index of plasma is mainly composed of two parts, one is the contribution of electrons, and the other is the contribution of ions and neutral atoms. Electrons and heavy particles have opposite contributions to the refractive index of plasma. The contribution of electrons to the refractive index makes the refractive index smaller, but the contribution of heavy particles to the refractive index makes the refractive index larger. Therefore, according to formula (3), when the contribution of electrons to the refractive index dominates, the phase shift is negative on the phase shift distribution. Conversely, when the contribution of the heavy particles to the refractive index dominates, the phase shift is positive on the phase shift distribution. From Fig. 5, we find that some areas have darker colors (positive phase shift) surrounding the arc channel boundary. The dense compressed air layer contains lots of neutral atoms. The air-spark switching plasma is generated between the electrodes and then expands into the surrounding air at supersonic speed, this will compress the surrounding air to form a dense compressed air layer. The dense compressed air layer shows a clear plasma boundary, so we can observe the plasma shape after complete diffusion.

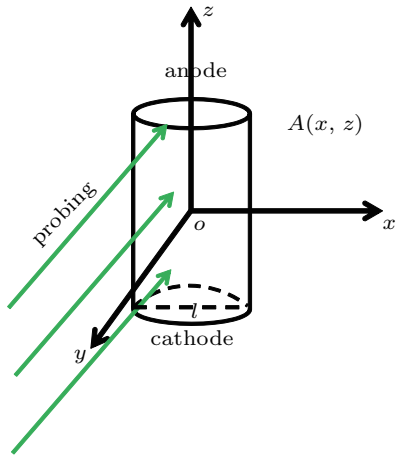


Fig. 4. Probing diagram of an arc channel in the air medium.

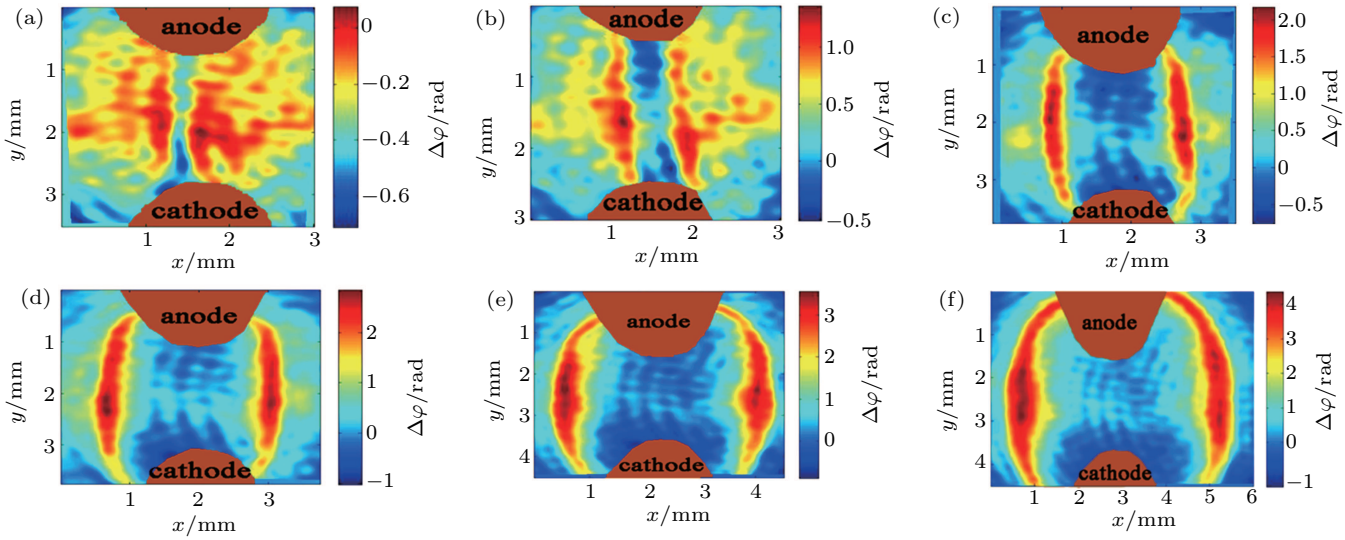


Fig. 5. Phase shift distribution of air-spark switch plasma obtained at different delay time: (a) 0 ns, (b) 10 ns, (c) 75 ns, (d) 130 ns, (e) 240 ns, (f) 420 ns. The phase shift $\Delta\varphi$ is expressed in radian.

4.3. Electron density distribution

For axisymmetric plasma systems, the inverse Abel transform is applied to calculate the 3D electron density distribution from the phase shift distribution. From Fig. 5, we can see that the air-spark switch plasma has good symmetry, so the inverse Abel transformation based on the Hanke–Fourier method[23] is applied to calculate the refractive index of the plasma. The result is shown in Fig. 6. Although the electron density in the arc channel is lower than 2×10^{19} cm^{-3}, we estimate the influence of the atom on the refractive index.[24] The estimation results show that the contribution of an electron to the refractive index is 1000 times that of an atom. Therefore, in the arc channel, the contribution from atoms to the refractive index is still negligible.

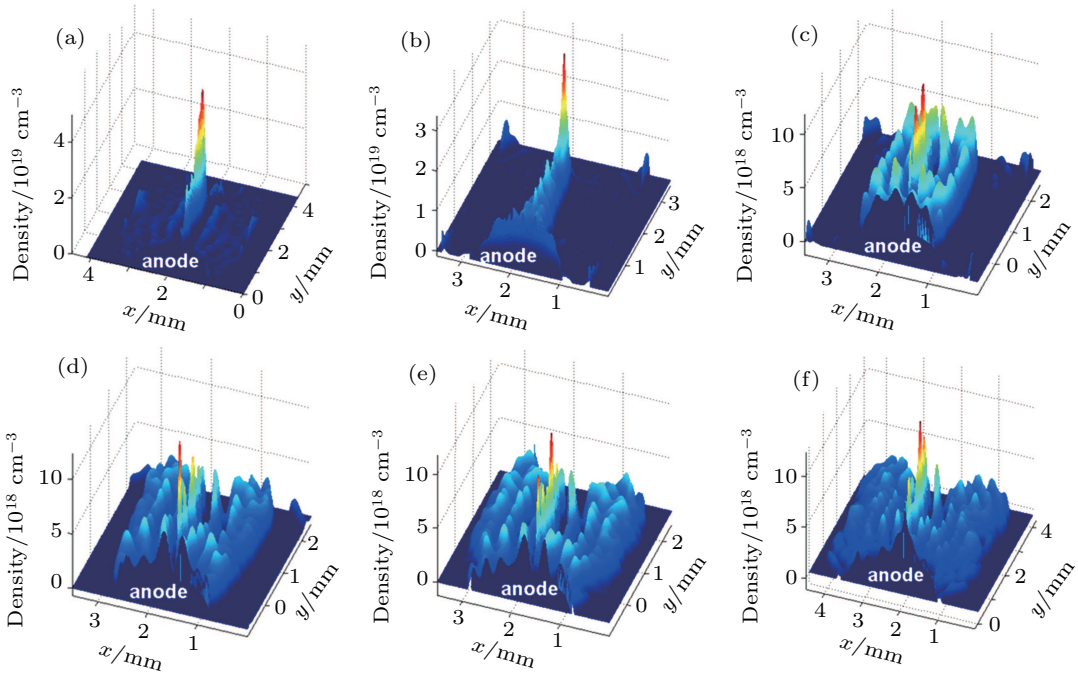


Fig. 6. The 3D electron density distribution extracted from the phase shift distribution at different delay time: (a) 0 ns, (b) 10 ns, (c) 75 ns, (d) 130 ns, (e) 240 ns, (f) 420 ns.

Figure 6 shows the temporal and spatial evolution of the air-spark switch plasma. In the initial discharge, at the tip of the cathode, the field emission provides the seed electrons for discharge. These seed electrons move toward the anode under the action of the electric field and collide with the background gas (air), producing a large amount of secondary electrons. The seed electrons and secondary electrons both move toward the anode and ionize the background gas under the action of the electric field. The electron avalanche effect causes a dense cloud of electrons formed near the cathode in a very short period of time. The electron cloud is shown in Fig. 7(b), the blue area near the cathode tip. Figure 7(b) indicates that the electron density near the cathode is higher than that near the anode in arc channel at the beginning of discharge. From Fig. 7(c), the electron density is up to 4.2×10^{19} cm^{-3} near the cathode, but the electron density near the anode is very small. The electron density distribution between the electrodes is shown in Fig. 7(c) and approximately fitted by a Boltzmann function (the red-solid line).

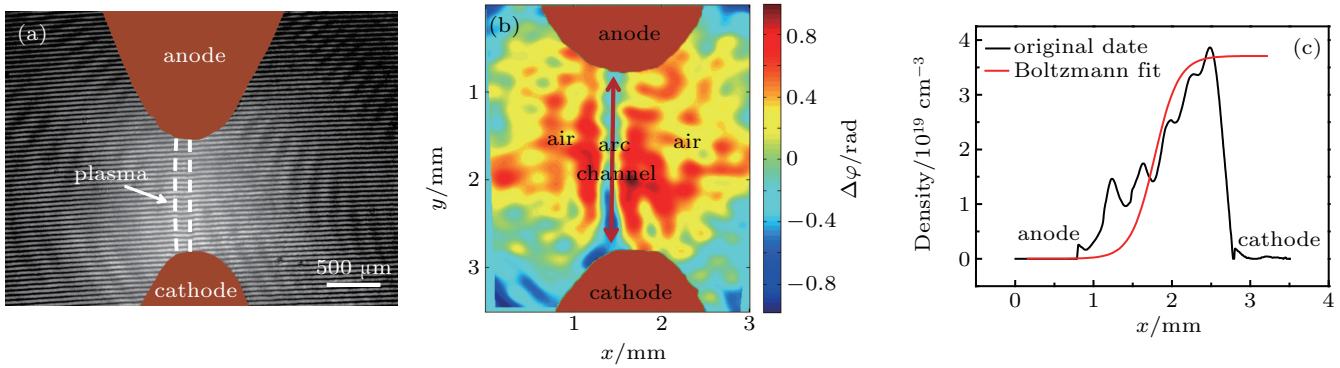


Fig. 7. Electron density distribution and phase shift distribution at the beginning of discharge ($t = 0$ ns) when the arc channel is just formed: (a) the interferogram, (b) the phase shift distribution, (c) the electron density distribution between the electrodes.

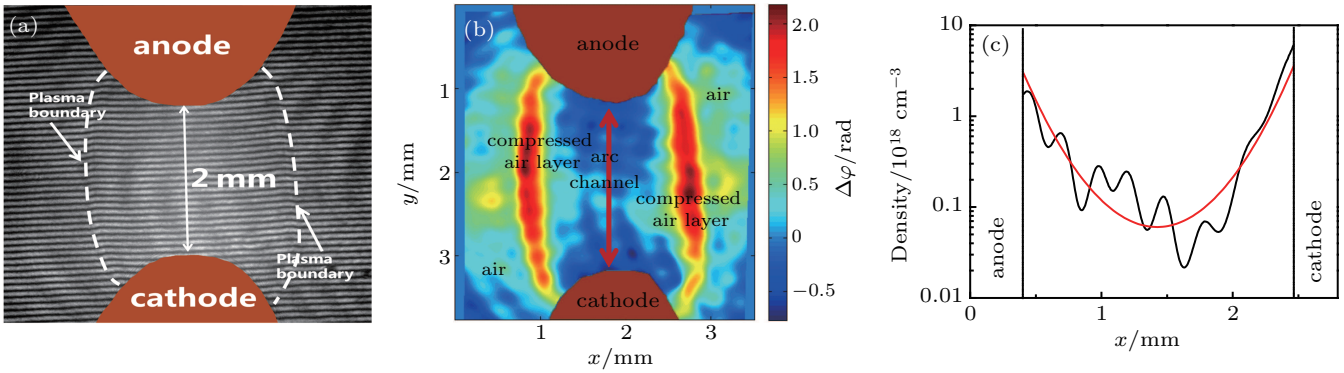


Fig. 8. Electron density distribution and phase shift distribution at $t = 75$ ns. The arc channel is completely formed at $t = 75$ ns. Two high-density areas of electrons are observed near the electrodes. The compressed air layers are observed due to the diffusion of the plasma. (a) The interferogram, (b) the phase shift distribution, (c) the electron density distribution between the electrodes.

The electrons accelerate toward the anode under the action of the electric field, and continuously ionize the neutral atom during the movement. The electron avalanche effect causes the arc channel to form quickly. So the initial plasma is generated in a short time. A large number of high-energy electron bombardment of the anode results in a large number of secondary electrons generated at the anode. The newly generated secondary electrons are attracted and accelerated by the anode, this results in more secondary electrons generated at the anode. So a dense electron cloud will form near the anode. Two high-density areas of electrons are observed near the electrodes when the arc channel is fully formed. This result is shown in Figs. 8(b) and 8(c). For the electron cloud near the cathode, there are three main sources of electrons: (i) the electrons from field emission, (ii) the secondary electrons from ionized neutral atoms, and (iii) the secondary electrons from ion bombardment cathode. For the electron cloud near the anode, there are also three main sources of electrons: (i) the electrons from field emission, (ii) the secondary electrons from ionized neutral atoms, and (iii) the secondary electrons from electron bombardment anode.

Intense collision and ionization lead to dense plasma generation during the formation of arc channels. This high temperature and high density plasma will expand into the air due to the pressure gradient in the plasma. The compressed air layer is generated because of the diffusion of the plasma, and is shown in Figs. 8(a) and 8(b). At the same time, this compressed air layer reveals the clear profile and diffusion radius of the plasma.

The plasma expanding into air is accompanied with the density decrease, the radius increase, and the temperature reduction. In our experiment, we select two reference locations, y_1 located near the cathode and y_2 located near the anode, as shown in Fig. 9(a). The distance between the reference position and the electrode tip is about 100 μm. Figure 9(b) shows the radial electron density distribution at $t = 0$ ns at y_1. The electron density profile is approximately fitted by a Gaussian function (the red-solid line). Figure 7(b) indicates that the arc channel is very narrow about 200 μm when it is just formed, but the electron density of the plasma is very high (4×10^{19} cm^{-3}) at position y_1. In the same manner, the radial distribution of electron density is obtained at different time, the result is shown in Fig. 10. Figures 10(a) and 10(b) show the evolution of electron density and radius of plasma with time at positions y_1 and y_2, respectively. Figure 10(a) shows that near the cathode, the electron density continues to decrease and the radius of plasma continues to increase due to the diffusion of the plasma. However, figure 10(b) shows that the electron density increases first and then decreases near the anode because of the formation of arc channels and subsequent diffusion of the plasma. The maximum density is up to 2.5×10^{19} cm^{-3} at $t = 75$ ns. The radius of plasma continues to increase near the anode.

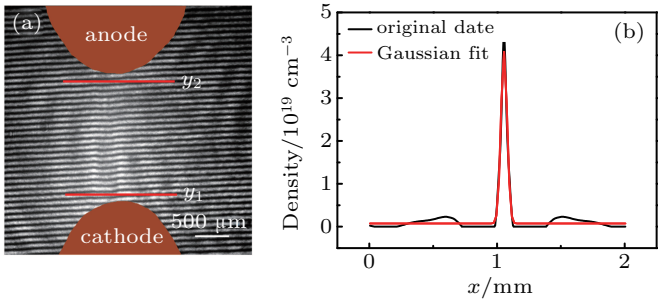


Fig. 9. Two reference locations y_1 and y_2, which are located near the electrodes. The distance between the reference position and the electrode tip is about 100 μm. (a) The interferogram obtained at $t = 0$ ns, and two reference locations y_1 and y_2 are illustrated with two red solid lines. (b) The radial electron density distribution at $t = 0$ ns at y_1.

Therefore, the working process of the air-spark switch can be described as follows: at the initial stage of discharge, the seed electrons are generated at the tip of the cathode by field emission. Under the action of the electric field, the seed electrons are accelerated to move toward the anode and ionize the background gas. So a large number of secondary electrons are produced. At this time, the electron density near the cathode is larger than that near the anode. The arc channel is rapidly formed due to the avalanche ionization mechanism. A large number of electrons bombard the anode and

produce more secondary electrons. Then, the electron density near the anode increases rapidly. So two high-density regions are formed near the cathode and anode. When the arc channel is fully formed, the plasma in the arc channel will expand into the air under the pressure gradient. As the diffusion progresses, the plasma density decreases, the radius increases and the temperature decreases. Finally, the plasma disappears into the air.

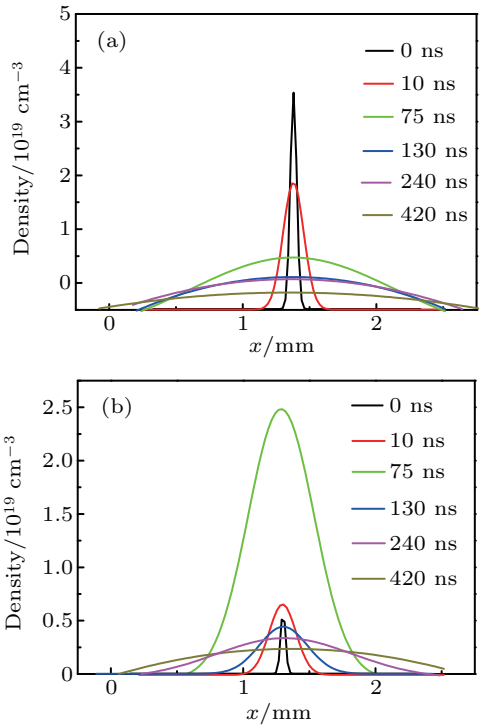


Fig. 10. Electron density distributions at different time superposed with Gaussian fit curves on a common radial coordinate system, which is center around the axes of the arc channels. (a) Electron density distributions at y_1 and (b) y_2.

5. Conclusion

Laser interferometry has an ultra-high spatial and temporal resolution, and is a powerful tool for studying plasma evolution. In this paper, we studied the working process of air-spark switches by laser interference technology. A series of interferograms that contain plasma information were obtained. The three-dimensional electron density distributions were obtained by numerical processing the interferograms. The electron density near the cathode up to 4.2×10^{19} cm^{-3} is higher than that near the anode in the arc channel at the beginning of discharge. Subsequently, the arc channel is rapidly formed under the action of the electric field. Due to the plasma expanding into air, the radius of the arc channel is increasing and the shock wave is formed in the front of the compressed air layer. The working process of the air-spark switch was described by analyzing the temporal and spatial evolution of the plasma electron density. The electron density near the anode increases first and then decreases, but the electron density near the cathode continues to decrease. The laser interferometry is demonstrated to be a valuable method to diagnose transient physical processes such as gas switching plasmas. The data of these experiments also provides a good reference for understanding the working process of the air-spark switch.

References

[1] Yalandin M I, Sharypov K A, Shpak V G, Shunailov S A and Mesyats G A 2010 *IEEE Trans. Dielectr Electr. Insul.* **17** 34
[2] Golnabi H 2000 *Rev. Sci. Instrum.* **71** 413
[3] Kefu L, Yaqing T, Liu X L and Jian Q 2013 *IEEE Trans. Electron. Devices* **60** 875
[4] Cheng X B, Liu J L and Qian B L 2010 *IEEE Trans. Plasma Sci.* **38** 516
[5] Rahaman H, Nam S H, Nam J W, Lee B J and Frank K 2010 *Appl. Phys. Lett.* **96** 141502
[6] Lee L, Cai L, Qi X D, Lin F C and Pan Y 2012 *J. Appl. Phys.* **111** 053306
[7] Kharlov A V 2010 *IEEE Trans. Plasma Sci.* **38** 2474
[8] Anaraki A P, Kadkhodapour J and Taherkhani B 2014 *J. Fai. L Anal. Preven.* **14** 784
[9] Inada Y, Matsuoka S, Kumada A, Ikeda H and Hidaka K 2012 *Phys. D: Appl. Phys.* **45** 435202
[10] Jiao Z H, Wang G L, Zhou X X, Wu C H, Zuo Y L, Zeng X M, Zhou K N and Su J Q 2016 *Plasma Sci. Technol.* **18** 1169
[11] Harilal S S, Brumfield B E and Phillips M C 2015 *Phys. Plasmas* **22** 063301
[12] Grun J, Stamper J, Manka C, Resnick J, Burris R, Crawford J and Ripin B H 1991 *Phys. Rev. Lett.* **66** 2738
[13] Zhang H C, Lu J and Ni X W 2009 *Opt. Commun.* **282** 1720
[14] Zhang H C, Lu J and Ni X W 2009 *J. Appl. Phys.* **106** 063308
[15] Harilal S S, Miloshevsky G V, Diwakar P K, LaHaye N L and Hassanein A 2012 *Phys. Plasmas* **19** 083504
[16] Yang Z F, Wu J and Wei W F 2016 *Phys. Plasmas* **23** 083523
[17] Weber B V and Fulghum S F 1997 *Rev. Sci. I Nstrum* **68** 1227
[18] Breitling D, Schittenhelm H, Berger P, Dausinger F and Hügel H 1999 *Appl. Phys. A: Mater. Sci. Process* **69** S505
[19] Alexander B, Burkhard J and Sergey P 2005 *IEEE Trans. Plasma Sci.* **5** 1465
[20] Ivanov V V and Anderson A A 2016 *Appl. Opt.* **55** 498
[21] Magesh T and John S 2008 *J. Appl. Phys.* **104** 013303
[22] Takeda M, Ina H and Kobayashi S 1982 *J. Opt. Soc. Am.* **72** 156
[23] Álvarez R, Rodero A and Quintero M C 2002 *Spectrochim. Acta Part. B At. Spectrosc.* **57** 1665
[24] Lu Y H, Wu J, Shi H T, Zhang D Y, Li X W, Jia S L and Qiu A C 2018 *Phys. Plasmas* **25** 072709